Strong-field Breit-Wheeler pair production in QED_{2+1}

A. Golub,[*] S. Villalba-Chávez,[†] and C. Müller[‡]

Institut für Theoretische Physik I, Heinrich-Heine-Universität Düsseldorf, Universitätsstraße 1, 40225 Düsseldorf, Germany

(Received 3 March 2021; accepted 18 March 2021; published 6 May 2021)

The Breit-Wheeler pair production process in $2+1$ dimensional spacetime is investigated. In the perturbative regime, nonvanishing rates at the energy threshold are found when odd numbers of photons take part in the reaction. This behavior is understood as a direct consequence of the reduced dimensionality and resembles a corresponding prediction made in gapped graphene monolayers. In the nonperturbative strong field regime, the effect of the dimensionality manifests itself in a different rate dependence on the quantum nonlinearity parameter. The consequence of this deviation is discussed briefly in line with the applicability of perturbation theory. We argue that, in addition to large values of the quantum nonlinearity parameter, the super-renormalizable character of quantum electrodynamics in $2+1$ dimensional spacetime might give rise to a breakdown of perturbation theory within certain energy scales.

DOI: 10.1103/PhysRevD.103.096002

I. INTRODUCTION

With the ongoing development of laser and accelerator infrastructures, the interest in producing electron-positron pairs from photon collisions has strongly grown over the last years as this process—despite being one of the most fundamental predictions of quantum electrodynamics (QED_{3+1})—has not been validated experimentally in full glory. After the pioneering work due to Breit and Wheeler on the pair production by the collision of two photons [1] (linear Breit-Wheeler process), further theoretical efforts revealed a phenomenology which manifests—among other issues—the nonlinear feature of QED_{3+1}. Initially, several authors considered interaction of light quanta with a plane-wave electromagnetic background [2–5]. Special attention has been paid to the perturbative [$\xi \ll 1$] and nonperturbative [$\xi \gg 1$] regimes defined by the intensity parameter of the involved laser wave $\xi = -\boldsymbol{e}E_0/(\omega m)$, with electron charge $\boldsymbol{e} < 0$, its mass m, frequency ω, and amplitude E_0 of the plane wave.[1] Besides, more elaborated treatments have been put forward in order to reach a more precise description of laser configurations [6–16], with particular emphasis on the highly nonlinear nonperturbative regime due to important links to a wider range of elusive phenomena [17–22]. Of special interest has been the region in which the quantum nonlinearity parameter $\chi = \xi kk'/m^2$—involving photon momenta k and k'—exceeds unity considerably as it might come accompanied with a breakdown of perturbation theory when $\alpha\chi^{2/3} \geq 1$ ($\alpha = \boldsymbol{e}^2/4\pi \approx 1/137$ is the fine structure constant) [23–31].

Despite the theoretical endeavor, experimental validation of Breit-Wheeler pair creation has, so far, been possible solely in the multiple-photon regime at $\xi \lesssim 1$ [32]. While this experiment provided important insights into this process, neither linear pair creation—for recent proposals see [33–38]—nor Breit-Wheeler pair creation at $\xi \gg 1$ has been observed by now. The reason why the former process is still elusive stems from the current limitations of reaching energetic photon beams with adequate intensities. Conversely, accessing the nonperturbative regime demands peak intensities $I = E_0^2 \sim I_c \approx 4.6 \times 10^{29}\ \mathrm{W\,cm^{-2}}$, corresponding to the Schwinger electric field scale $E_c \approx 1.3 \times 10^{16}\ \mathrm{V\,cm^{-1}}$ in the relevant frame of reference. Reaching this condition requires ultrahigh laser intensities $I \sim (10^{21} - 10^{24})\ \mathrm{W\,cm^{-2}}$ in the laboratory frame in conjunction with a beam of sufficiently energetic γ photons, which represents a hard challenge to overcome (for recent proposals, see [39,40]).

A low-energy test ground for yet unobserved QED_{3+1} processes is provided by band-gapped graphene monolayers. In this two dimensional honeycomb of carbon atoms, charge carriers near the degeneracy points possess a Dirac-like dispersion relation with the speed of light replaced by the Fermi velocity $v_F \approx 1/300$. Hence, their behavior can be effectively described by a $2+1$

[*]Alina.Golub@uni-duesseldorf.de
[†]selym@tp1.uni-duesseldorf.de
[‡]c.mueller@tp1.uni-duesseldorf.de

[1]From now on, we use a metric with signature $\mathrm{diag}(g^{\mu\nu}) = (1,-1,-1)$. Throughout, a natural unit system where $c = \hbar = 1$ is adopted.

dimensional Dirac model and the interband transition of electrons, i.e., the production of electron-hole pairs, can be exploited as a toy model for addressing QED_{3+1} pair production-related questions. This idea has motivated investigations of analogs to the Schwinger mechanism [41,42] by delivering inherent insights caused by the low-dimensional material: The power of the preexponential factor is changed from 2 in QED_{3+1} to $3/2$ in graphene. Likewise, band-gapped graphene has been presented as a suitable material to simulate the Breit-Wheeler process with two (linear case) and three photons [43]. In the latter case, as in the studies linked to the Schwinger-like mechanism, inherent properties due to the low-dimensional character of the medium came to a scene. Contrary to QED_{3+1}, the rate linked to this process does not vanish at the energy threshold. This poses special feature questions, whether its occurrence extends to perturbative Breit-Wheeler reactions in which more than three photons are absorbed and to which extent the Lorentz symmetry breaking caused by the Fermi velocity takes part in its realization. Addressing these questions is not an easy task within the Dirac model, mainly because the dispersive properties of the medium make the theoretical treatment difficult to handle.[2]

Against this background, we study in the present paper the Breit-Wheeler pair production in $2+1$ dimensional quantum electrodynamics (QED_{2+1}) in various interaction regimes from weak to very strong fields. In particular, we show that the threshold lifting persists in this Lorentz invariant framework when an odd number of photons are absorbed, confirming that this phenomenon results as an inherent consequence of the reduced spacetime dimensionality. Besides, we reveal characteristic influences of the dimensionality on the nonperturbative production rates for both small and large values of the quantum nonlinearity parameter and discuss the implications for a breakdown of perturbation theory in this scenario.

Considerations of low-dimensional scenarios have proven useful in various areas of physics. They revealed, for example, valuable insights on nonperturbative aspects of QCD (see, e.g., [44] and references therein) and even provided a solvable quantum field theory model for gravity [45]. Investigations of the Chern-Simons term—intrinsically linked to QED_{2+1} [46]—have improved our understanding of the high temperature behavior of QED_{3+1}, leading, in addition, to an accurate description of the quantum Hall effect [47]. Likewise, various research on the subject of Schwinger pair creation in arbitrary spacetime dimensions has been performed by considering different field configurations such as constant uniform electric and magnetic fields [48] and electric fields of finite duration [49]. Regarding Breit-Wheeler pair production, a recent study based on a model Hamiltonian in one spatial dimension has allowed for spacetime resolution of this process [50]. Moreover, the accuracy of predictions from an intrinsically one-dimensional QED theory when applied to a highly symmetric system in $3+1$ dimensions was studied [51].

Another important area of applicability for lower dimensional theories is the field of quantum simulation. Gradually, this branch is gaining interest as it enables one to simulate the behavior of various many-body ensembles via ultracold atom systems placed in sophisticated optical lattices. Because of a complex technical implementation, these quantum simulators have been restricted so far to systems of lower dimensionality, so the question arises of which differences occur as compared to $3+1$ dimensions. In the realm of quantum electrodynamics, the progress in this field has led to an experimental implementation of the $1+1$-dimensional Schwinger mechanism [52,53], which was investigated thoroughly by theoreticians [54–56], whereas current research efforts are spent toward QED_{2+1} [57–60]. Hence, with the present study of the nonperturbative Breit-Wheeler pair creation, we provide a scenario that may be further explored through the branch of quantum simulation.

Our paper is organized as follows: In Sec. II, we introduce Volkov states in QED_{2+1} and apply them in Sec. III to obtain a general expression of the Breit-Wheeler pair production rate. Afterward, in Sec. IV, we evaluate the rate numerically in various intensity regimes and support this analysis by an asymptotic study. Our conclusions are given in Sec. V, while in Appendix A, we briefly review the Breit-Wheeler rates in $3+1$ dimensions, and the two-photon pair production process is described in the lowest order of perturbation theory in Appendix B.

II. VOLKOV STATES IN 2+1 DIMENSIONS

In a $2+1$ dimensional spacetime, the time evolution of planar relativistic electrons interacting with an electromagnetic field $a_\mu(x)$ is described by the Dirac equation,

$$(i\not{D} - m)\psi = 0, \tag{1}$$

which manifests a $\mathrm{SO}(1,2)$ invariance [61,62]. In this expression, $\psi(x)$ stands for a two component spinor wave function, whereas $\not{D} \equiv \gamma^\mu D_\mu$ and $D_\mu = \partial_\mu + iea_\mu$ refers to the covariant derivative, with $e<0$ denoting the electric charge in $2+1$ dimensions. Observe that the latter notation differs from the one used in the introduction ($\boldsymbol{e}$). The reason behind this change will be discussed below. The γ^μ matrices linked to this low-dimensional scenario are determined by Pauli matrices $\gamma^\mu = (\sigma_3, i\sigma_2, -i\sigma_1)$ and are also constricted by the Clifford algebra $\{\gamma^\mu, \gamma^\nu\} = 2g^{\mu\nu}\mathbb{1}_{2\times 2}$, with $\mu = 0, 1, 2$.

[2]As a consequence of the asymmetry introduced by the simultaneous appearance of the Fermi velocity and the speed of light, solutions to the Dirac equation of graphene in the field of a plane wave are much more difficult to obtain than in QED_{3+1}.

As in $3+1$ dimensions, the solvability of Eq. (1) is restricted to a certain class of electromagnetic fields. Here, we will focus on the solution resulting when $a^\mu(x)$ is chosen as a polarized plane-wave-like three-potential,

$$a^\mu(kx) = a_0 \epsilon^\mu \cos(kx), \tag{2}$$

characterized by the amplitude a_0, the wave vector $k^\mu = (\omega, \vec{k})$, and a transverse polarization ϵ^μ $[\epsilon^\mu k_\mu = 0]$, which is normalized according to $\epsilon^\mu \epsilon_\mu = -1$. We remark that in $2+1$ dimensions, the magnetic field provided by $a^\mu(x)$ is a pseudoscalar, whereas the electric field is a two component vector. It is worth emphasizing that the field in Eq. (2) is supposed to be a solution of a Maxwell equation without taking the Chern-Simons contribution into account, an assumption that applies whenever the energy-momentum transfer is much larger than the topological mass of the gauge field.

Despite the inherent differences caused by the dimensionality, the procedure for establishing the $2+1$ dimensional Volkov-states does not differ much from the well-known approach in QED_{3+1} (see, for instance, Refs. [3,63,64]). In line, we find

$$\begin{aligned}\psi_{p^-}(x) = \sqrt{\frac{m}{q_0^- A}}\left(1 + \frac{e}{2kq^-}\not{k}\not{a}\right) u_{p^-} \\ \times \exp\left[-iq^- x - i\frac{ea_0 q^- \epsilon}{kq^-}\sin(kx)\right. \\ \left. - i\frac{e^2 a_0^2}{8kq^-}\sin(2kx)\right].\end{aligned} \tag{3}$$

The state given above has been normalized in such a way that the time averaged electron density $\langle j^0 \rangle = \langle \bar{\psi}_{p^-} \gamma^0 \psi_{p^-} \rangle$ with $\bar{\psi}_{p^-} \equiv \psi^\dagger_{p^-} \gamma^0$ amounts to one particle in the normalization area A. While u_{p^-} refers to a free spinor $[a_\mu = 0]$ with positive energy, the quantity $q^-_\mu = p^-_\mu + \frac{e^2 a_0^2}{4kp^-} k_\mu$ stands for an averaged effective electron momentum with $kp^- = kq^-$, $\epsilon p^- = \epsilon q^-$, where the electron momentum is denoted by p^-. Moreover, the Volkov solution for a positron $\psi_{p^+}(x)$ can be read off from Eq. (3) by carrying out the replacements, $p^- \to -p^+$ and $u_{p^-} \to v_{p^+}$, where v_{p^+} is the free negative-energy solution. Both spinors u_{p^-} and v_{p^+} are normalized in accordance with the following rules:

$$u_{p^-}\bar{u}_{p^-} = \frac{\not{p}^- + m}{2m}, \qquad v_{p^+}\bar{v}_{p^+} = \frac{\not{p}^+ - m}{2m} \tag{4}$$

and $\bar{u}_{p^-}\gamma_\mu u_{p^-} = p^-_\mu/m$ for $\bar{u}_{p^-} \equiv u^\dagger_{p^-}\gamma^0$, $\bar{v}_{p^+} \equiv v^\dagger_{p^+}\gamma^0$.

III. BREIT-WHEELER PAIR CREATION IN QED_{2+1}

A. General considerations

In QED_{2+1}, the reduction of space dimensions gives rise to changes in the physical dimensions of the involved fields ψ, a_μ, and the electric charge e,

$$[\psi] = \mathcal{E}, \quad [a] = \mathcal{E}^{1/2} \quad \text{and} \quad [e] = \mathcal{E}^{1/2}, \tag{5}$$

where $\mathcal{E}$ stands for the dimension of energy. As the charge in the equation above has a positive energy dimension, QED_{2+1} belongs to the class of super-renormalizable theories. This fact prevents us from identifying $e^2/4\pi$ with the traditional fine-structure constant $\alpha \approx 1/137$ and demands one to look for an adequate dimensionless parameter from which a perturbative treatment can be justified.

In the scope of the strong-field Breit-Wheeler process, two gauge fields are involved in the pair creation: a strong field a_μ and a low-intensity field a'_μ. Hence, we can identify dimensionless[3] intensity parameters $\eta = -ea_0/m > 0$ and $\eta' = -ea'_0/m > 0$, where a_0 and a'_0 stand for the field amplitudes, and perform the perturbative expansion in η', assuming that $\eta' \ll 1$.

Accordingly, our starting point is the generic transition amplitude for the Breit-Wheeler process [see Fig. 1],

$$S_{fi} = -ie \int d^3x \bar{\psi}_{p^-}(x) \not{a}'(x) \psi_{p^+}(x), \tag{6}$$

where $a'_\mu(x) = \frac{a'_0}{2}\epsilon'_\mu e^{-ik'x}$ denotes the photon wave function, which refers to the amplitude a'_0 rather than being normalized to one particle in the area, and the polarization ϵ'_μ satisfies the conditions $\epsilon' k' = 0, \epsilon'\epsilon' = -1$, with $k'^\mu = (\omega', \vec{k}')$.[4] In this expression, $\psi_{p^-}(x)$ and $\psi_{p^+}(x)$ stand for the Volkov solutions as given in Sec. II.

However, we point out that the applicability of Eq. (6) also depends on the regime dictated by η, where additional specification of the expansion parameters may be in order. Indeed, as it happens in QED_{3+1}, large values of $\eta \gg 1$ might compensate the smallness of η', making the effective coupling strength far from being perturbative. In this scenario, the effect of radiative corrections should be

[3] It is worth remarking that, in a minimally coupled framework, the combination $ea_0^{(\prime)}$ has always a dimension of energy regardless the number of space dimensions d: $[ea_0^{(\prime)}] = \mathcal{E}^{(3-d)/2}\mathcal{E}^{(d-1)/2} = \mathcal{E}$.

[4] As will be seen below, the pair production rate depends on the Lorentz invariant product kk'. In most studies of the strong-field Breit-Wheeler process conducted so far, a counterpropagating beam geometry (maximizing $kk' = 2\omega\omega'$) has been considered, with $\omega' \gg m \gg \omega$ in view of the experimental capabilities.

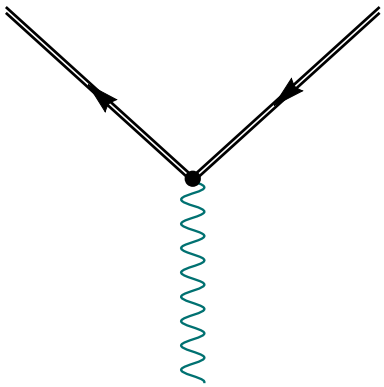

FIG. 1. Feynman diagram of the Breit-Wheeler pair creation process in a plane-wave background. Here, the wavy line represents a quantized photon, whereas the solid double lines stand for Volkov states of electron and positron.

included in the transition amplitude. Further discussion on this topic will follow at the end of Sec. IV B.

To evaluate the integral in Eq. (6), we follow the usual procedure and introduce a Fourier expansion of an exponential,

$$\mathrm{e}^{-iz_-\sin(kx)-iz_+\sin(2kx)}=\sum_{n=-\infty}^{\infty}\mathrm{e}^{-inkx}\tilde{J}_n(z_-,z_+), \tag{7}$$

in which the generalized Bessel function is defined as an infinite sum of a product of ordinary Bessel functions of one argument [3,65,66],

$$\tilde{J}_n(z_-,z_+)=\sum_{m=-\infty}^{\infty}J_{n-2m}(z_-)J_m(z_+), \tag{8}$$

and write ($l=1,2$),

$$\begin{aligned}\cos^l(kx)\mathrm{e}^{-iz_-\sin(kx)-iz_+\sin(2kx)}&=\sum_{n=-\infty}^{\infty}\mathrm{e}^{-inkx}\tilde{\mathcal{J}}_n^l,\\ \tilde{\mathcal{J}}_n^1&\equiv\frac{1}{2}[\tilde{J}_{n+1}(z_-,z_+)+\tilde{J}_{n-1}(z_-,z_+)],\\ \tilde{\mathcal{J}}_n^2&\equiv\frac{1}{4}[\tilde{J}_{n+2}(z_-,z_+)+2\tilde{J}_n(z_-,z_+)+\tilde{J}_{n-2}(z_-,z_+)].\end{aligned} \tag{9}$$

By exploiting these definitions, we can write Eq. (6) as

$$\begin{aligned}S_{fi}=&-i\frac{ea_0'}{2}\sqrt{\frac{m^2}{q_0^+q_0^-A^2}}\sum_{n=-\infty}^{\infty}(2\pi)^3\delta_{nk+k',q^++q^-}\\&\times\bar{u}_{p^-}M_nv_{p^+},\end{aligned} \tag{10}$$

where $\delta_{x,y}\equiv\delta^3(x-y)$, and M_n is of the following form:

$$\begin{aligned}M_n=&\not{\epsilon}'\tilde{J}_n+\frac{ea_0}{2}\tilde{\mathcal{J}}_n^1\left(\frac{\not{\epsilon}\not{k}\not{\epsilon}'}{kq^-}-\frac{\not{\epsilon}'\not{k}\not{\epsilon}}{kq^+}\right)\\&-\frac{e^2a_0^2}{2kq^+kq^-}\epsilon'^{\mu}k_{\mu}\tilde{\mathcal{J}}_n^2\not{k}.\end{aligned} \tag{11}$$

Notice that energy-momentum conservation $q^++q^-=nk+k'$, anticommutativity of gamma matrices, and transversal condition have been employed, and the arguments of generalized Bessel functions read $z_-=ea_0(\frac{q^+\epsilon}{q^+k}-\frac{q^-\epsilon}{q^-k})$, $z_+=-\frac{e^2a_0^2}{8}\frac{kk'}{kq^+kq^-}$. Next, we consider the differential rate of pair creation per area defined as

$$dR=\frac{|S_{fi}|^2}{TA}A^2\frac{d^2q^-}{(2\pi)^2}\frac{d^2q^+}{(2\pi)^2}. \tag{12}$$

Here, the phase space is expressed in terms of the effective particle momenta, in accordance with the normalization chosen in Eq. (3). When inserting Eq. (10) into the equation above, we end up with

$$\begin{aligned}dR=&\frac{e^2a_0'^2m^2}{8\pi}\sum_{n=-\infty}^{\infty}|\bar{u}_{p^-}M_nv_{p^+}|^2\\&\times\delta_{nk+k',q^++q^-}\frac{d^2q^-}{q_0^-}\frac{d^2q^+}{q_0^+},\end{aligned} \tag{13}$$

where the sum over n can be interpreted as a sum over a number of absorbed photons from the classical field $a^{\mu}(kx)$. Furthermore, the square of the amplitude $|\mathcal{M}^n|^2=|\bar{u}_{p^-}M_nv_{p^+}|^2$ can be written as

$$|\mathcal{M}^n|^2=\mathrm{Tr}\left[\frac{\not{p}^-+m}{2m}M_n\frac{\not{p}^+-m}{2m}\bar{M}_n\right], \tag{14}$$

with $\bar{M}_n=\gamma^0M_n^{\dagger}\gamma^0$. To show the relation above, the properties of free Dirac spinors in $2+1$ dimensions given in Eq. (4) were used. It is interesting to point out that, although the form of the squared amplitude remains unchanged as compared to $3+1$ dimensions, the trace is no longer taken over a 4×4 matrix but over one of the dimension 2×2. This feature is responsible for introducing major differences with respect to QED_{3+1}.[5]

Additionally, since the gauge field in $2+1$ dimensions has only one transverse polarization direction, we can make use of the relation,

$$\epsilon'^{\mu}\epsilon'^{\nu}=-g^{\mu\nu}-\frac{k'^{\mu}k'^{\nu}-n'k'(k'^{\mu}n'^{\nu}+k'^{\nu}n'^{\mu})}{(n'k')^2}, \tag{15}$$

[5]In the calculations, we have used

$$\begin{aligned}\gamma^0\gamma^{\dagger\mu}\gamma^0=\gamma^{\mu},\gamma^{\mu}\gamma_{\mu}=3\mathbb{1}_{2\times2},\mathrm{Tr}[\gamma^{\mu}\gamma^{\nu}]=2g^{\mu\nu},\\ \mathrm{Tr}[\gamma^{\mu}\gamma_{\mu}]=6,\gamma^{\mu}\gamma^{\nu}\gamma_{\mu}=-\gamma^{\nu},\mathrm{Tr}[\gamma^{\nu}]=0,\\ \mathrm{Tr}[\gamma^{\mu}\gamma^{\nu}\gamma^{\alpha}]=-2i\epsilon^{\mu\nu\alpha},\gamma^{\mu}\gamma^{\nu}\gamma^{\alpha}\gamma_{\mu}=4g^{\nu\alpha}-\gamma^{\nu}\gamma^{\alpha},\\ \gamma^{\mu}\gamma^{\nu}\gamma^{\alpha}\gamma^{\beta}\gamma_{\mu}=\gamma^{\nu}\gamma^{\alpha}\gamma^{\beta}-2\gamma^{\beta}\gamma^{\alpha}\gamma^{\nu},\\ \mathrm{Tr}[\gamma^{\mu}\gamma^{\nu}\gamma^{\alpha}\gamma^{\beta}]=2(g^{\mu\nu}g^{\alpha\beta}-g^{\mu\alpha}g^{\nu\beta}+g^{\mu\beta}g^{\nu\alpha}),\end{aligned}$$

with Levi-Civita tensor $\epsilon^{\mu\nu\alpha}$ with $\epsilon^{012}=1$.

where $n'^{\mu}=(1,0,0)$. It is worth emphasizing that, owing to the Ward identity, only the term containing $-g^{\mu\nu}$ will contribute to the squared amplitude. Having these properties in mind, we arrive at

$$|\mathcal{M}^n|^2=\tilde{J}_n^2-\frac{e^2a_0^2}{m^2}\left(1-\frac{(kk')^2}{4kq^+kq^-}\right)[(\tilde{\mathcal{J}}_n^1)^2-\tilde{J}_n\tilde{\mathcal{J}}_n^2], \tag{16}$$

where the energy-momentum balance and transversal condition ($k\epsilon=0$) have been used. We remark that, when deriving this formula, the following relation was exploited [3,65]:

$$(n+2z_+)\tilde{J}_n-z_-\tilde{\mathcal{J}}_n^1-4z_+\tilde{\mathcal{J}}_n^2=0. \tag{17}$$

Inserting Eq. (16) into Eq. (13), the rate for Breit-Wheeler pair creation in $2+1$ dimensions reads,

$$dR=\frac{e^2a_0'^2m^2}{8\pi}\sum_{n\geq n_0}^{\infty}\delta_{nk+k',q^++q^-}\frac{d^2q^-}{q_0^-}\frac{d^2q^+}{q_0^+}\times\left[\tilde{J}_n^2-\eta^2\left(1-\frac{(kk')^2}{4kq^+kq^-}\right)[(\tilde{\mathcal{J}}_n^1)^2-\tilde{J}_n\tilde{\mathcal{J}}_n^2]\right]. \tag{18}$$

The fact that the summation index starts at $n_0=2m_*^2/(kk')$, with $m_*^2=m^2(1+\eta^2/2)=q^{\pm 2}$ referring to the effective electron mass, is understood here as a consequence of the energy-momentum balance. Leaving aside the lower dimensionality of the delta functions and the involved integration measures, the main source of difference between dR and the unpolarized rate in $3+1$ dimensions [see Eq. (A3) in Appendix A] lies in the precise structure of the squared amplitude [compare with Eq. (16)]. It resembles the squared amplitude of the pair production by a photon with polarization parallel to the electric field of the wave [as given in Eqs. (A1) and (A2)]. This fact highlights the restriction provided by a lower dimensionality: Both photon wave vectors and polarizations are bound to a plane. Hence, when moving the system to a center-of-momentum frame, where photons are counterpropagating, their polarizations have to be parallel.

In order to highlight the consequences linked to the spacetime dimensionality further, we change the integration variables to a set referred to as the center of momentum of the created particles, where $\vec{q}^-=-\vec{q}^+=-\vec{q}$, $n\vec{k}=-\vec{k}'$, $n\omega=\omega'$. Afterward, q^- is integrated out, and the remaining integral is expressed in polar coordinates,

$$R=\frac{e^2a_0'^2m^2}{8\pi}\sum_{n\geq n_0}^{\infty}\int_0^{2\pi}d\phi\int_0^{\infty}\frac{dq}{2q_0}\delta(q-q_n^*)\times\left(\tilde{J}_n^2-\eta^2\left(1-\frac{1}{1-\frac{q^2}{\omega'^2}\cos^2(\phi)}\right)[(\tilde{\mathcal{J}}_n^1)^2-\tilde{J}_n\tilde{\mathcal{J}}_n^2]\right), \tag{19}$$

when setting $|\vec{q}|\equiv q$, $kq^+=\omega[\omega'-q\cos(\phi)]$, $kq^-=\omega[\omega'+q\cos(\phi)]$, $\epsilon q^-=-\epsilon q^+=q\sin(\phi)$, and $q_n^*=\sqrt{\omega'^2-m_*^2}$, $q_0=\omega'$. Additionally, we introduce a Mandelstam invariant $s=\sqrt{kk'/2m^2}$, which allows us to write $q_n^*=\omega'\sqrt{1-(1+\eta^2/2)/ns^2}$. Requiring that the number of absorbed photons exceeds a critical number $n\geq(1+\eta^2/2)/s^2$, we obtain for every value of n a threshold energy $s^2\geq(1+\eta^2/2)/n=s_n^2$, which must be overpassed so that the process takes place.

B. Threshold behavior

Now, we are interested in investigating the behavior of the rate at the energy threshold, where the particles are created with zero momentum ($q=0$). It is noteworthy that at the threshold, the integral over the phase space will not always vanish and is governed solely by the form of the amplitude. This fact represents a crucial difference to the $3+1$ dimensional case where, after integrating over q^- in the center-of-momentum frame, the remaining integral $\int\frac{d^3q}{q_o^2}\delta(2q_0-2\omega')\propto q_n^*$ always goes to zero at the threshold. Therefore, we focus on the behavior of the process amplitude. In this context, the arguments of the generalized Bessel functions in the center-of-momentum frame read,

$$z_-=-\frac{2\eta}{ms^2}\frac{q\sin(\phi)}{1-\frac{q^2}{\omega'^2}\cos^2(\phi)}\overset{s\to s_n}{\to}0, \tag{20}$$

$$z_+=-\frac{\eta^2}{4s^2}\frac{1}{1-\frac{q^2}{\omega'^2}\cos^2(\phi)}\overset{s\to s_n}{\to}-\frac{\eta^2}{4s_n^2}\equiv z_{+n}, \tag{21}$$

and, consequently, the generalized Bessel function at the threshold can be written as [65,66]

$$\tilde{J}_n(0,z_{+n})=\begin{cases}J_{n/2}(z_{+n}), & n\text{ even},\\ 0, & n\text{ odd}.\end{cases} \tag{22}$$

Hence, when an even number of strong field photons $n=2\ell$ is absorbed, the rate [see Eq. (19)] at the threshold behaves as

$$R_{s\to s_n}=\frac{e^2a_0'^2m}{8}\sum_{2\ell\geq n_0}^{\infty}\frac{J_\ell^2(-\frac{\eta^2\ell}{2(1+\eta^2/2)})}{1+\eta^2/2}. \tag{23}$$

While this expression tends to vanish as η grows ($\eta\gg 1$), the contribution for $\eta\ll 1$ approximates

$$R_{s\to s_n}^{\eta\ll 1}\approx\frac{e^2a_0'^2m}{8}\sum_{2\ell\geq n_0}^{\infty}\eta^{4\ell}\frac{\ell^{2(\ell-1)}}{2^{4\ell}\Gamma^2(\ell)}, \tag{24}$$

where $\Gamma(x)$ stands for the gamma function [67]. We see that the rate above does not vanish. This causes a lifting of the

rate at each threshold when an even number of strong field photons is absorbed, which resembles the behavior at low intensity of the Breit-Wheeler process in graphene [43]. Our analysis indicates that this peculiarity is a general consequence of the $2+1$ dimensionality and does not rely on the Lorentz invariance breakdown that is caused by the Fermi velocity of this medium.

IV. ASYMPTOTIC STUDY

This section is devoted to establishing asymptotic expressions of the Breit-Wheeler pair creation rate [see Eq. (18)] for different intensity parameters of the strong field η.

A. Behavior for $\eta \ll 1$

For small laser parameter $\eta \ll 1$, the leading order contribution of Eq. (18) results, when energetically allowed, from the absorption of a single laser photon ($n=1$). A representative Feynman diagram for this process is depicted in the upper panel of Fig. 2. In this limiting case, the effective electron and positron momenta can be simply taken as $q^{\pm}=p^{\pm}$ so that the arguments of the generalized Bessel functions read as $z_{-}=\eta m(\frac{p^{-}\epsilon}{p^{-}k}-\frac{p^{+}\epsilon}{p^{+}k})$, $z_{+}=-\frac{\eta^2 m^2}{8}\frac{kk'}{kp^{+}kp^{-}}$. Their respective proportionality on η and η^2 allows us to expand the Bessel functions (see Appendix C in [65]),

$$\tilde{J}_n(\eta\beta,\eta^2\varrho)\approx\left(\frac{\eta^2\varrho}{2}\right)^{\frac{n}{2}}\times\begin{cases}\sum_{k=0}^{n/2}\frac{(\beta^2/2\varrho)^k}{(2k)!(n/2-k)!} & \text{for even } n,\\ \sum_{k=0}^{(n-1)/2}\frac{(\beta^2/2\varrho)^{k+1/2}}{(2k+1)!((n-1)/2-k)!} & \text{for odd } n,\end{cases} \tag{25}$$

where the shorthand notation $\beta=m(\frac{p^{-}\epsilon}{p^{-}k}-\frac{p^{+}\epsilon}{p^{+}k})$, $\varrho=-\frac{m^2}{8}\frac{kk'}{kp^{+}kp^{-}}$ has been introduced. Hence, in the lowest order in η, the squared amplitude can be written as

$$|\mathcal{M}^{n=1}_{\eta\ll1}|^2=\frac{\eta^2\beta^2}{4}-\frac{\eta^2}{4}\left(1-\frac{(kk')^2}{4kp^{+}kp^{-}}\right). \tag{26}$$

The use of Eq. (15) in combination with the energy-momentum balance $p^{+}+p^{-}=k+k'$ allows us to express the differential rate of the pair production in the following form:

$$dR^{n=1}_{\eta\ll1}=\frac{e^2a_0'^2m^2}{8\pi}\delta_{k+k',p^{+}+p^{-}}|\mathcal{M}^{n=1}_{\eta\ll1}|^2\frac{d^2p^{-}d^2p^{+}}{p_0^{-}p_0^{+}},$$
$$|\mathcal{M}^{n=1}_{\eta\ll1}|^2=\frac{\eta^2}{4}\left[\frac{(kk')^2}{4kp^{+}kp^{-}}-1+\frac{2m^2kk'}{kp^{+}kp^{-}}-\frac{m^4(kk')^2}{(kp^{+}kp^{-})^2}\right]. \tag{27}$$

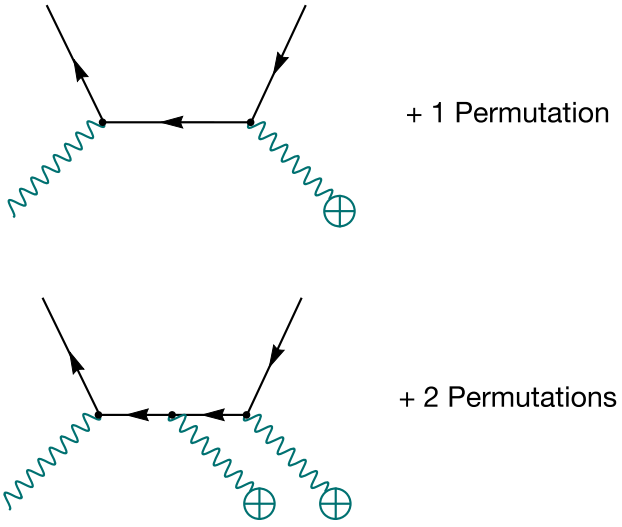

FIG. 2. Feynman diagrams of two (upper panel) and three (lower panel) photons pair creation processes. In both panels, free fermions are represented by external solid lines, and internal lines stand for the free fermion propagators, while wavy lines correspond to photons stemming from quantized and classical sources (the latter are marked by crossed circles).

It is worth mentioning that this expression coincides with the outcome resulting from perturbation theory when the classical field in Eq. (1) is canonically quantized (see details in Appendix B).

Finally, we integrate the rate in Eq. (27) by adopting polar coordinates. To facilitate the integrations over the momenta, we go over to the center-of-momentum frame, where $\vec{p}=\vec{p}^{+}=-\vec{p}^{-}$, $p_0^{+}=p_0^{-}$, $\omega=\omega'$, $kk'=2\omega\omega'=2\omega^2$, and $kp=\omega(p_0-|\vec{p}|\cos(\phi))$. Then, after integrating out p^{-} and p_0 we arrive at

$$R^{n=1}_{\eta\ll1}=\frac{e^2a_0'^2m^2}{8\pi}\frac{\eta^2}{4}\frac{1}{2\omega}\int_0^{2\pi}d\phi\left[-1-\frac{4u^2}{[1-(1-u)\cos^2(\phi)]^2}+\frac{(1+4u)}{[1-(1-u)\cos^2(\phi)]}\right], \tag{28}$$

with $u=m^2/\omega^2$. The remaining integration can be performed analytically by using Eqs. (3.616.8) and (3.642.3) in Ref. [68],

$$R^{n=1}_{\eta\ll1}=\frac{e^2a_0'^2m}{8\pi}\frac{\pi\eta^2}{4s}\left[-1-\frac{2(s^2+1)}{s^3}+\frac{(4+s^2)}{s}\right], \tag{29}$$

where the result has been expressed in terms of the Mandelstam variable $s=\sqrt{kk'/2m^2}$. Observe that in this context, the energy threshold translates into $s\geq1$. We remark that for $s=1$, the rate above vanishes. In the upper panel of Fig. 3, a comparison between the asymptotic

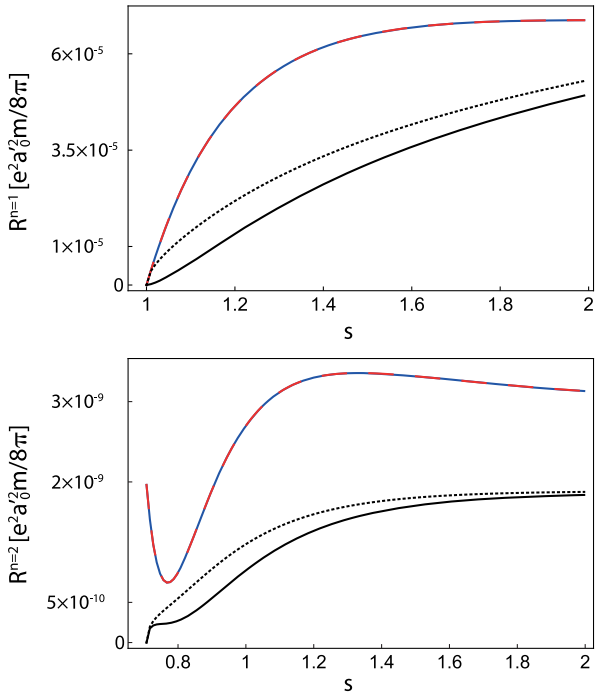

FIG. 3. Dependence of the pair production rate in $2+1$ dimensions on the Mandelstam invariant s for $\eta = 0.01$. In the upper panel, the numeric evaluation of the $n = 1$ summand of Eq. (18) is depicted in blue, and the corresponding asymptotic expression [see (29)] is colored in red. For comparison, the QED_{3+1} rates for unpolarized, and parallel polarized photons [3] are shown in black solid and black dotted lines, correspondingly. In the lower panel, we compare the outcome of Eq. (31) with the numerically evaluated summand for $n = 2$ of Eq. (18), using the same color scheme as in the upper picture.

expression in Eq. (29) (red dashed line) and the numerical evaluation for $n = 1$ in Eq. (18) (blue curve) is depicted. This assessment has been done by taking $\eta = 0.01$. For further comparison, Fig. 3 exhibits the behavior of the corresponding process in $3+1$ dimensions colored in black. While the solid line results from an unpolarized photon beam, the dotted one refers to the case of parallel polarization.

Usually, the derivation of the linear Breit-Wheeler rate is performed within the second order of perturbation theory when considering two quantized photons (see Appendix B). To bring Eq. (29) into the corresponding form, the replacements $a_0^{(\prime)2} \equiv 2/\omega^{(\prime)}A$ need to be done. This way, the quantity $\alpha_{2+1} = e^2/(4\pi m)$ appears in the rate, which is the counterpart of the fine structure constant in QED_{3+1}. We remark that α_{2+1} plays the role of a perturbative coupling constant, provided $m \gg e^2/(4\pi)$.

Next, we consider the case where two strong field photons are absorbed ($n = 2$) [see lower panel of Fig. 2 for the corresponding Feynman diagram]. The leading order contribution to this process is described by the amplitude,

$$|\mathcal{M}^{n=2}_{\eta\ll 1}|^2 = \left(\frac{\eta^2\varrho}{2} + \frac{\eta^2\beta^2}{8}\right)^2 - \frac{\eta^2}{4}\left(1 - \frac{(kk')^2}{4kp^+kp^-}\right)\left(\frac{\eta^2\beta^2}{8} - \frac{\eta^2\varrho}{2}\right), \quad (30)$$

where the involved Bessel functions were expanded with help of Eq. (25). Furthermore, we perform the integration in the center-of-momentum frame, which is defined similarly to the case $n = 1$, taking into account that $\omega' = 2\omega$. Consequently, the asymptote of the three-photon reaction reads,

$$R^{n=2}_{\eta\ll 1} = \frac{e^2 a_0'^2 m}{8\pi}\frac{\pi\eta^4}{128 s^8}[10 - 30s^2 + 19s^4 + 12s^8]. \quad (31)$$

We note that at the threshold $s = s_2 = \sqrt{1/2}$, the expression above coincides with the outcome resulting from Eq. (24) for $n = 2$, providing a nonzero contribution. This effect can be seen in the lower panel of Fig. 3, where the asymptote as given in the equation above is depicted in blue, whereas the red dashed curve results from evaluating Eq. (18) for $n = 2$. These outcomes are compared with the QED_{3+1} rates for unpolarized photon (black solid) and photon polarized parallel to the classical field (black dotted), which vanish at the threshold.

Finally, we remark that the fact that η and η' are dimensionless regardless of the spacetime dimension would allow us to transfer our predictions for the production rate from the $2+1$ dimensional model to a real situation once it is assumed that they coincide with those defined from the physical charge and amplitude in $3+1$ dimensions, *i.e.*, if $\eta = \xi$. Observe that, identifying alternatively α_{2+1} with $\alpha \approx 1/137$ makes the rate a function depending explicitly on the field amplitude in $2+1$ dimensions. However, the dimension of this quantity $[a_0] = \mathcal{E}^{1/2}$ differs from the one of its $3+1$ dimensional counterpart $\sim\mathcal{E}$, preventing, this way, a mutual matching and so, a direct link with physical quantities.

B. Behavior for $\eta \gg 1$

Contrary to the previous case of small laser parameters, for $\eta \gg 1$, a large number of summands in Eq (18) will provide non-negligible contributions to the rate. Indeed, a huge amount of photons is needed for the process to take place so that a transition to the continuum limit $\sum_n \ldots \to \int dn \ldots$ can be developed.[6] Afterward, n together with $\vec{q}^+$ are integrated out by using the delta functions. Consequently, Eq. (18) reduces to

[6]Actually, the transition is made on the variable $\mathfrak{s}_n \equiv n/(1+\eta^2/2) = 1/s_n^2$, for which the interval between two neighbor terms converges to zero $\Delta\mathfrak{s}_n = (1+\eta^2/2)^{-1} \to d\mathfrak{s}$ as $\eta \to \infty$.

$$R_{\eta\gg1} = \frac{e^2 a_0'^2 m^2}{8\pi}\int \frac{d^2q^-}{q_0^- k q^+}|\mathcal{M}_{\eta\gg1}^{n=n^*}|^2. \tag{32}$$

Here, $|\mathcal{M}_{\eta\gg1}^{n=n^*}|^2$ is given in Eq. (16), where $n \to n^*$ and $n^* = q^- k'/[\omega(\omega' - k_2' - q_0^- + q_2^-)]$. We assume without loss of generality that the strong field a^μ is polarized in x_1- direction. Next, let us introduce new variables,

$$\mathcal{X} = \frac{kq^+}{m^2}\eta, \qquad \mathcal{X}' = \frac{kq^-}{m^2}\eta, \qquad \gamma^- = q_0^- - q_2^-. \tag{33}$$

Observe that these definitions allow us to write $z_\pm$ [see below Eq. (7)] in the following form:

$$z_+ = -\frac{\eta^3\kappa}{8\mathcal{X}\mathcal{X}'}, \qquad z_- = \frac{\eta^2}{m\mathcal{X}\mathcal{X}'}(q^-\epsilon\mathcal{X} - q^+\epsilon\mathcal{X}'), \tag{34}$$

where the quantum nonlinearity parameter in $2+1$ dimensions $\kappa = \eta k k'/m^2$ has been introduced. Further, we perform a substitution $q_2^- \to \gamma^-$, which allows us to write the integral in Eq. (32) as

$$R_{\eta\gg1} = \frac{e^2 a_0'^2 m^2}{8\pi}\frac{\eta}{m^2}\int_{-\infty}^{\infty}\frac{dq_1^-}{\mathcal{X}}\int_0^\lambda \frac{d\gamma^-}{\gamma^-}|\mathcal{M}_{\eta\gg1}^{n=n^*}|^2, \tag{35}$$

where $\lambda = \omega' - k_2'$, and

$$|\mathcal{M}_{\eta\gg1}^{n=n^*}|^2 = \tilde{J}_{n^*}^2 - \eta^2\left(1 - \frac{\kappa^2}{4\mathcal{X}\mathcal{X}'}\right)[(\tilde{\mathcal{J}}_{n^*}^1)^2 - \tilde{J}_{n^*}\tilde{\mathcal{J}}_{n^*}^2]. \tag{36}$$

The matrix element above still contains generalized Bessel functions. In order to proceed, we have calculated their asymptotic expansions in the relevant limits,[7] following the lines of Appendix B in Ref. [3] and paying special attention to modifications arising from the reduced dimensionality. It turns out that the latter induces some minor changes but does not affect the derivations substantially. Having this in mind, we find that for $\eta \gg 1$ and $\eta \gg \kappa^{1/3}$, the square of the matrix element approximates

$$|\mathcal{M}_{\eta\gg1}^{n=n^*}|^2 \approx \frac{2}{\pi}\left(-\frac{1}{4z_+\sin^2(x_0)}\right)^{2/3} \times\left[\Phi^2(z) - \left(1 - \frac{\kappa^2}{4\mathcal{X}\mathcal{X}'}\right)\left(\Phi^2(z) + \frac{\Phi'^2(z)}{z}\right)\right], \tag{37}$$

[7]In order to exploit the large argument behavior, the Bessel functions are written in their integral representation $\tilde{J}_n(z_-, z_+) = \frac{1}{\pi}\mathrm{Re}[\int_0^\pi d\theta e^{f(\theta)}]$, with $f(\theta) = -iz_-\sin(\theta) - iz_+\sin(2\theta) + in\theta$, and the integration is performed asymptotically via the method of steepest descent [69] by expanding $f(\theta)$ around the saddle point. Since we are interested in deriving asymptotic formulas for both $\kappa \ll 1$ and $\kappa \gg 1$, an expansion up to the third order term is needed [70].

with $z = \frac{(-4\sin^2(x_0)z_+)^{2/3}}{\eta^2\sin(x_0)}$. Moreover, $\Phi(z)$ stands for the Airy function [3]. Observe that in the equation above, a new substitution involving x_0 was introduced: $\cos(x_0) = -\frac{\omega}{\kappa m^3}(q_1^-\gamma^+ - q_1^+\gamma^-)$, with $\gamma^+ = q_0^+ - q_2^+$, $\gamma^+ + \gamma^- = \lambda$ and $x_0 \in [0,\pi]$. Furthermore, we substitute $\mathcal{X}' = \frac{\eta\omega}{m^2}\gamma^-$ and define $\mathcal{X}' = \frac{\kappa}{2}[1 + \tanh(\vartheta)]$, $\mathcal{X} = \frac{\kappa}{2}[1 - \tanh(\vartheta)]$. Notice that the integral over $\mathcal{X}'$ is defined over the interval $[0,\kappa]$. As the integrand is symmetric in $\mathcal{X}'$ and $\mathcal{X}$ with $\mathcal{X}' + \mathcal{X} = \kappa$, we can write $\int_0^\kappa d\mathcal{X}'\ldots = 2\int_0^{\kappa/2} d\mathcal{X}'\ldots$. Therefore, the integration over ϑ will run from 0 to ∞. Having these in mind, we obtain

$$R_{\eta\gg1} \approx \frac{e^2 a_0'^2 m}{8\pi}\frac{8}{\pi}\int_0^{\pi/2} dx_0\int_0^\infty \frac{d\vartheta}{\mathrm{ch}^2(\vartheta)}\sqrt{z} \times\left[\Phi^2(z) + \mathrm{sh}^2(\vartheta)\left(\Phi^2(z) + \frac{\Phi'^2(z)}{z}\right)\right], \tag{38}$$

with $z = \left(\frac{2\mathrm{ch}^2(\vartheta)}{\kappa\sin(x_0)}\right)^{2/3}$. We remark that using the relations $\Phi'^2(z)/z = 1/(2z)d^2\Phi^2(z)/dz^2 - \Phi^2(z)$ and $\Phi^2(z) = \frac{1}{2^{2/3}\sqrt{\pi}}\int_0^\infty \frac{dt}{\sqrt{t}}\Phi(t + 2^{2/3}z)$, combined with the defining equation for the Airy functions [71], allows us to write the rate as a function depending linearly on the Airy function of shifted argument $t + 2^{2/3}z$,

$$R_{\eta\gg1} \approx \frac{e^2 a_0'^2 m}{8\pi}\frac{8}{2^{2/3}\pi^{3/2}}\int_0^{\pi/2} dx_0\int_0^\infty \frac{dt}{\sqrt{t}} \times\int_0^\infty \frac{d\vartheta\sqrt{z}}{\mathrm{ch}^2(\vartheta)}\left(1 + \frac{2^{1/3}\mathrm{sh}^2(\vartheta)}{z}\right)\Phi(t + 2^{2/3}z). \tag{39}$$

For derivation of asymptotes, we come back to Eq. (38) and start with considering $\kappa \ll 1$. Since the Airy functions decrease monotonically, the largest contribution to the integral in Eq. (38) results from the region close to $\tilde{\vartheta} = 0$ and $\tilde{x}_0 = \pi/2$. Hence, we expand Φ and Φ' for large arguments as $1/\kappa \gg 1$,

$$\Phi^2(z) = \frac{z}{3\pi}K_{1/3}^2\left(\frac{2}{3}z^{3/2}\right) \overset{z\to\infty}{\to} \frac{z^{-1/2}}{4\pi}e^{-\frac{4}{3}z^{3/2}}, \tag{40}$$

$$\Phi'^2(z) = \frac{z^2}{3\pi}K_{2/3}^2\left(\frac{2}{3}z^{3/2}\right) \overset{z\to\infty}{\to} \frac{z^{1/2}}{4\pi}e^{-\frac{4}{3}z^{3/2}}, \tag{41}$$

with the modified Bessel functions of the second kind $K_\nu(x)$ [67]. Taking into account the expansions above, we further expand all involved functions in $\tilde{\vartheta}$ and $\tilde{x}_0$ and perform the remaining integrations, ending up with

$$R_{\eta\gg1,\kappa\ll1} \approx \frac{e^2 a_0'^2 m}{8\pi}\frac{3\kappa}{8\sqrt{2}}e^{-\frac{8}{3\kappa}}. \tag{42}$$

Comparing the equation above with its $3+1$ dimensional analog [as given in Eq. (A4) in Appendix A], we see that the power linked to the quantum nonlinearity parameter κ in the preexponential factor is equal to 1 rather than $3/2$. This difference comes from the reduced dimensionality of the phase space: Similarly, as in QED_{3+1}, the integrand in this limit depends on κ solely through the exponential function $e^{-\frac{4}{3z}^{3/2}}$, and integration over each variable provides a factor $\kappa^{1/2}$. Since in $2+1$ dimensions z does not depend on a variable responsible for a dimension orthogonal to the plane spanned by photon polarization and propagation vectors, we obtain a power of $1/2$ less in the quantum nonlinearity parameter than in $3+1$ dimensions.

Establishment of the asymptotic formula for $\kappa \gg 1$ demands a more elaborated procedure. To this end, we substitute $\kappa \sin(x_0) = p$ and $\mathrm{ch}(\vartheta) = u$ in Eq. (38),

$$R_{\eta\gg1,\kappa\gg1} \approx \frac{e^2 a_0'^2 m}{8\pi}\frac{16}{3\pi^2}\int_0^\kappa \frac{dp}{p\sqrt{\kappa^2-p^2}}\int_1^\infty \frac{du}{\sqrt{u^2-1}} \times \left[u^2 K_{1/3}^2\left(\frac{4u^2}{3p}\right) + (u^2-1)K_{2/3}^2\left(\frac{4u^2}{3p}\right)\right], \tag{43}$$

and split the integration over p into two intervals: $[0, p_0]$ and $[p_0, \kappa]$, with $p_0 \ll \kappa$. Then, the contribution from the first interval will be negligible as it scales with κ^{-1},

$$\int_0^{p_0} \frac{dp}{p\sqrt{\kappa^2-p^2}}\ldots \approx \frac{1}{\kappa}\int_0^{p_0}\frac{dp}{p}\ldots \sim \frac{p_0^{4/3}}{\kappa} \ll 1. \tag{44}$$

For the extant integral, we perform a transition to a new variable $t = 4u^2/3p$, whereas p remains unchanged. As a consequence,

$$R_{\eta\gg1,\kappa\gg1} \approx \frac{e^2 a_0'^2 m}{8\pi}\frac{4}{\sqrt{3}\pi^2}\int_{p_0}^\kappa \frac{dp}{\sqrt{p}\sqrt{\kappa^2-p^2}}\int_{\frac{4}{3p}}^\infty dt \times \left[\frac{3p}{4}\sqrt{\frac{t}{\frac{3pt}{4}-1}}K_{1/3}^2(t) + \sqrt{\frac{\frac{3pt}{4}-1}{t}}K_{2/3}^2(t)\right]. \tag{45}$$

At this point, it is suited to split the integration over t into two sectors:

$$\int_{4/3p}^\infty dt\ldots = \int_{4/3p}^{t_0} dt\ldots + \int_{t_0}^\infty dt\ldots. \tag{46}$$

Here, the parameter t_0 satisfies the conditions $4/3\kappa \ll 4/3p_0 \ll t_0 \ll 1, 3\kappa t_0/4 \gg 3p_0 t_0/4 \gg 1$. Let us consider firstly the contribution defined over $[t_0, \infty]$. In this region, $3pt/4 \gg 1$ holds, and we obtain approximately

$$\int_{t_0}^\infty dt\ldots \approx \int_{t_0}^\infty dt\sqrt{\frac{3p}{4}}(K_{1/3}^2(t)+K_{2/3}^2(t)) \approx \sqrt{\frac{3p}{4}}\frac{3\Gamma^2(\frac{2}{3})}{2^{2/3}t_0^{1/3}}, \tag{47}$$

where the smallness of t_0 has been used [$t_0 \ll 1$], and $\Gamma(x)$ denotes the gamma function [67].

Now, let us turn our attention to the contribution in Eq. (46) defined over $[4/3p, t_0]$. As in this interval $t \ll 1$, we can use the small argument behavior of the modified Bessel functions $K_\nu(t) \approx \Gamma(\nu)/2(t/2)^\nu$ [67] and, consequently, perform the integration over t. Taking advantage of the fact that $4/3pt_0 \ll 1$ and $t_0 \ll 1$, we arrive at

$$\int_{4/3p}^{t_0} dt\ldots \approx -\sqrt{\frac{3p}{4}}\frac{3\Gamma^2(\frac{2}{3})}{2^{2/3}t_0^{1/3}} + \frac{3^{5/6}\sqrt{\pi}}{2^{10/3}}\frac{\Gamma^2(\frac{2}{3})\Gamma(\frac{1}{3})}{\Gamma(\frac{11}{6})}p^{5/6} + \frac{3^{1/6}\sqrt{\pi}}{2^{5/3}}\frac{\Gamma^2(\frac{1}{3})\Gamma(-\frac{1}{3})}{\Gamma(\frac{1}{6})}p^{1/6}. \tag{48}$$

We combine both Eqs. (47) and (48) in Eq. (46). As a consequence, t_0 drops out as it should, and the resulting expression is inserted into Eq. (45). Hence, to the leading order in κ, we obtain

$$R_{\eta\gg1,\kappa\gg1} \approx \frac{e^2 a_0'^2 m}{8\pi}\frac{3^{11/6}}{2^{1/3}5\pi}\Gamma^2\left(\frac{2}{3}\right)\kappa^{1/3}. \tag{49}$$

As for the case $\kappa \ll 1$, a deviation with respect to QED_{3+1} occurs. Indeed, the presence of the $\kappa^{1/3}$ dependence is in sharp contrast to the well-established $\chi^{2/3}$ behavior so that the rate in $3+1$ dimensions manifests [for comparison, see Eq. (A5) in Appendix A]. It provides the first evidence that the proper expansion parameter for QED_{2+1} in the strong field [see Eq. (1)] could be $g \sim \alpha_{2+1}\kappa^{1/3}$ whenever $g \ll 1$. However, at this point, this statement must be considered as a conjecture; its confirmation will require a more elaborative investigation of consecutive terms within the perturbative expansion [28–31]. While this analysis is beyond the scope of the present study, some interesting consequences can be anticipated owing to the super-renormalizable feature of the theory. Firstly, upon identifying $\kappa \sim \chi \gg 1$, the presence of the $1/3$ exponent would induce a breakdown of perturbation theory softer than in strong-field QED_{3+1} if $\alpha_{2+1} \sim \alpha$. However, if $\alpha_{2+1} \gg \alpha\kappa^{1/3}$, *i.e.*, for a mass scale of the electric charge $e^2/(4\pi) \gg m\alpha\kappa^{1/3}$, this breakdown in QED_{2+1} could be stronger than in QED_{3+1}.

The result of this section is summarized in Fig. 4, which shows the dependence of R on the quantum nonlinearity parameter κ (blue solid line). This figure depicts, in addition, the asymptotes for small κ (purple dotted line)

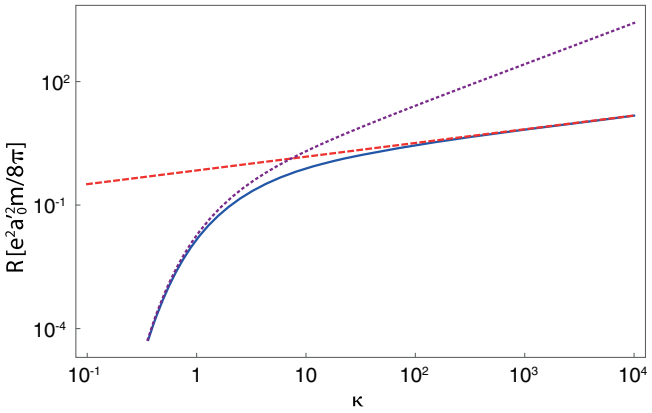

FIG. 4. Dependence of the Breit-Wheeler pair production rate in QED_{2+1} on the quantum nonlinearity parameter κ (blue solid line) at asymptotically large value of η. The corresponding behavior of R for $\kappa \ll 1$ [see Eq. (42)] and $\kappa \gg 1$ [see Eq. (49)] are plotted in purple dotted and red dashed lines, respectively.

and large κ (red dashed line) given in Eqs. (42) and (49), correspondingly.

V. CONCLUSION

In the present work, we have investigated the Breit-Wheeler pair creation in $2+1$ dimensional Minkowski space. Special attention was paid to the domains of small and large intensity parameter η. We have shown that the dimensionality plays a crucial role when considering the process rates, leading to surprising differences when comparing them to the $3+1$ dimensional case. We have found that for $\eta \ll 1$, the low dimensionality causes nonvanishing contributions to the rate at the threshold when an even number of strong field photons is absorbed. This outcome supports and extends the results obtained in a recent study on band-gapped graphene [43]. As this feature persists in a Lorentz invariant vacuum, we conclude that in a honeycomb of carbon atoms, it occurs independently of the medium.

In the high intensity regime ($\eta \gg 1$), the $2+1$ dimensionality induces changes in the pair production rate, which are manifested through a dependence on the quantum nonlinearity parameter κ different from the one appearing within the pure QED_{3+1} context. On the basis of this finding, we have argued that the so far accepted criteria within the strong field QED_{3+1} community on the applicability of perturbation theory might be subject to modifications as the spacetime dimensionality changes. Indeed, we have seen that the super-renormalizable character of QED_{2+1} constitutes an aspect to take into account in this regard because, once the electron mass becomes smaller than the energy scale linked to the square of the electric charge, the effective fine-structure constant is no longer a small parameter, and a breakdown of perturbation theory could take place even for quantum nonlinearity parameter of the order of unity.

ACKNOWLEDGMENTS

This work has been funded by the Deutsche Forschungsgemeinschaft (DFG) under Grant No. 416699545 within the Research Unit FOR 2783/1 and Grant No. 388720772 (MU 3149/5-1).

APPENDIX A: STRONG-FIELD BREIT-WHEELER PROCESS IN QED_{3+1}

Following [3], the differential pair production rate per volume in QED_{3+1} for a linearly polarized strong laser field reads,

$$dR_{\perp,\parallel}^{3+1} = \frac{\mathbf{e}^2 m^2}{8\omega' V \pi^2} \sum_{n \geq n_0}^{\infty} \delta_{nk+k'.q^+ + q^-} \frac{d^3q^-}{q_0^-} \frac{d^3q^+}{q_0^+} w_{\perp,\parallel}, \tag{A1}$$

with

$$w_{\parallel} = \sigma \tilde{J}_n^2 - \xi^2 \left(1 - \frac{(kk')^2}{4kq^+kq^-}\right)[(\tilde{\mathcal{J}}_n^1)^2 - \tilde{J}_n \tilde{\mathcal{J}}_n^2],$$
$$w_{\perp} = (1-\sigma)\tilde{J}_n^2 + \xi^2 \frac{(kk')^2}{4kq^+kq^-}[(\tilde{\mathcal{J}}_n^1)^2 - \tilde{J}_n \tilde{\mathcal{J}}_n^2], \tag{A2}$$

and $\sigma = -\xi^2(\frac{z_-^2}{64z_+^2} + \frac{1}{2} + \frac{n}{4z_+})$. Here, the subscripts $\parallel, \perp$ denote the cases of parallel and perpendicular polarization of the quantized photon, respectively, when compared to the polarization of the strong field. Notice that in $2+1$ dimensions for counterpropagating photons, only parallel alignment is allowed, and $\sigma = 1$ holds. When taking this point into account, one finds the similarity of $dR_{\parallel}^{3+1}$ with Eq. (18) when adjusting the prefactors ($1/2\omega' V \equiv \mathbf{a}_0'^2/4$, with $\mathbf{a}_0'$ denoting the field amplitude in 3+1 dimensions), the dimension of the delta function, substituting the four vectors with three vectors, and ξ with η. Usually, in $3+1$ dimensions, one averages over the polarizations of quantized photons obtaining the unpolarized differential rate per volume,

$$dR^{3+1} = \frac{1}{2}\left(dR_{\perp}^{3+1} + dR_{\parallel}^{3+1}\right). \tag{A3}$$

In the limit $\xi \gg 1$, we find { see Eqs. (36') and (36") in Ref. [3]} for $\chi \ll 1$,

$$R_{\parallel}^{3+1} = \frac{3\mathbf{e}^2 m^2}{32\omega' V}\left(\frac{\chi}{2\pi}\right)^{3/2} \mathrm{e}^{-8/(3\chi)}, \quad R_{\perp}^{3+1} = 2R_{\parallel}^{3+1}, \tag{A4}$$

and

$$R_{\parallel}^{3+1} = \frac{27\Gamma^7(\frac{2}{3})\mathbf{e}^2 m^2}{56\pi^5 \omega' V}\left(\frac{3\chi}{2}\right)^{2/3}, \quad R_{\perp}^{3+1} = \frac{3}{2}R_{\parallel}^{3+1} \tag{A5}$$

for $\chi \gg 1$. The expressions above are to be compared with their $2+1$ dimensional analogs in Eqs. (42) and (49).

APPENDIX B: PAIR CREATION BY TWO PHOTONS IN 2+1 DIMENSIONS

In $2+1$ dimensions, the S-matrix element that describes the electron positron pair creation out of two photons looks similar to its counterpart in QED_{3+1},

$$S_{fi} = -\frac{ie^2}{A^2}\sqrt{\frac{m^2}{p_0^+ p_0^-}}\sqrt{\frac{1}{2^2\omega\omega'}}(2\pi)^3\delta_{k+k',p^++p^-}\mathcal{M}_p, \tag{B1}$$

with

$$\mathcal{M}_p = \bar{u}_{p^-}\left(\frac{\not{\epsilon}\not{\epsilon}'}{\not{k}'-\not{p}^+-m+i0}+\frac{\not{\epsilon}'\not{\epsilon}}{\not{k}-\not{p}^+-m+i0}\right)v_{p^+}. \tag{B2}$$

Here, the fermion propagator in $2+1$ dimensions reads,

$$S_F(x-y) = \int\frac{d^3p}{(2\pi)^3}\frac{e^{ip(x-y)}}{\not{p}-m+i0}.$$

The probability rate associated with the perturbative pair creation results from Eq. (12) when substituting $q^- \to p^-$ and $q^+ \to p^+$. Explicitly,

$$dR_{\gamma\gamma'} = \frac{e^4}{A^2}\frac{m^2}{8\pi\omega\omega'}\delta_{k+k',p^++p^-}|\mathcal{M}_p|^2\frac{d^2p^-}{p_0^-}\frac{d^2p^+}{p_0^+}, \tag{B3}$$

where the square of the S-matrix element is

$$\begin{aligned}|\mathcal{M}_p|^2 &= \frac{1}{16m^2}\mathrm{Tr}\left[\left(\not{\epsilon}\frac{\not{k}'-\not{p}^++m}{k'p^+}\not{\epsilon}'+\not{\epsilon}'\frac{\not{k}-\not{p}^++m}{kp^+}\not{\epsilon}\right)(\not{p}^+-m)\right.\\ &\left.\times\left(\not{\epsilon}'\frac{\not{k}'-\not{p}^++m}{k'p^+}\not{\epsilon}+\not{\epsilon}\frac{\not{k}-\not{p}^++m}{kp^+}\not{\epsilon}'\right)(\not{p}^-+m)\right].\end{aligned} \tag{B4}$$

Using the properties of the gamma matrices (see footnote 5) and the energy-momentum conservation, the expression above reduces to

$$|\mathcal{M}_p|^2 = \frac{1}{m^2}\left[\frac{(kk')^2}{4kp^+kp^-}-1+\frac{2m^2kk'}{kp^+kp^-}-\frac{m^4(kk')^2}{(kp^+kp^-)^2}\right]. \tag{B5}$$

We note that the form of $|\mathcal{M}_p|^2$ differs from its $3+1$ dimensional counterpart (see [72]). When inserting Eq. (B5) into Eq. (B3), we obtain the differential rate,

$$\begin{aligned}dR_{\gamma\gamma'} = \frac{e^4a_0^2a_0'^2}{32\pi}\delta_{k+k',p^++p^-}\frac{d^2p^-}{p_0^-}\frac{d^2p^+}{p_0^+}\\ \times\left[\frac{(kk')^2}{4kp^+kp^-}-1+\frac{2m^2kk'}{kp^+kp^-}-\frac{m^4(kk')^2}{(kp^+kp^-)^2}\right],\end{aligned} \tag{B6}$$

where the relation $a_0^{(\prime)2} \equiv 2/\omega^{(\prime)}A$ has been used. This expression coincides with Eq. (27), provided the intensity parameter $\eta = ea_0/m$ is identified.

[1] G. Breit and J. A. Wheeler, Collision of two light quanta, Phys. Rev. **46**, 1087 (1934).
[2] H. R. Reiss, Absorption of light by light, J. Math. Phys. (N.Y.) **3**, 59 (1962).
[3] A. I. Nikishov and V. I. Ritus, Quantum processes in the field of a plane electromagnetic wave and in a constant field. I, Zh. Eksp. Teor. Fiz. **46**, 776 (1964) [Sov. Phys. JETP **19**, 529 (1964)].
[4] A. I. Nikishov and V. I. Ritus, Pair production by a photon and photon emission by an electron in the field of an intense electromagnetic wave and in a constant field. I, Zh. Eksp. Teor. Fiz. **52**, 1707 (1967) [Sov. Phys. JETP **25**, 1135 (1967)].
[5] V. I. Ritus, Quantum effects of the interaction of elementary particles with an intense electromagnetic field, J. Russ. Laser Res. **6**, 497 (1985).
[6] F. Ehlotzky, K. Krajewska, and J. Z. Kamiński, Fundamental processes of quantum electrodynamics in laser fields of relativistic power, Rep. Prog. Phys. **72**, 046401 (2009).
[7] A. Di Piazza, C. Müller, K. Z. Hatsagortsyan, and C. H. Keitel, Extremely high-intensity laser interactions with fundamental quantum systems, Rev. Mod. Phys. **84**, 1177 (2012).
[8] N. B. Narozhny and A. M. Fedotov, Extreme light physics, Contemp. Phys. **56**, 249 (2015).
[9] T. Heinzl, A. Ilderton, and M. Marklund, Finite size effects in stimulated laser pair production, Phys. Lett. B **692**, 250 (2010).
[10] K. Krajewska and J. Z. Kamiński, Breit-Wheeler process in intense short laser pulses, Phys. Rev. A **86**, 052104 (2012).
[11] A. I. Titov, H. Takabe, B. Kämpfer, and A. Hosaka, Enhanced Subthreshold e^+e^- Production in Short Laser Pulses, Phys. Rev. Lett. **108**, 240406 (2012).
[12] A. I. Titov, B. Kämpfer, A. Hosaka, T. Nousch, and D. Seipt, Determination of the carrier envelope phase for short, circularly polarized laser pulses, Phys. Rev. D **93**, 045010 (2016).

[13] M. J. A. Jansen and C. Müller, Strong-field Breit-Wheeler pair production in short laser pulses: Identifying multiphoton interference and carrier-envelope-phase effects, Phys. Rev. D **93**, 053011 (2016).
[14] A. Di Piazza, Nonlinear Breit-Wheeler Pair Production in a Tightly Focused Laser Beam, Phys. Rev. Lett. **117**, 213201 (2016).
[15] Q. Z. Lv, S. Dong, Y. T. Li, Z. M. Sheng, Q. Su, and R. Grobe, Role of the spatial inhomogeneity on the laser-induced vacuum decay, Phys. Rev. A **97**, 022515 (2018).
[16] A. Hartin, A. Ringwald, and N. Tapia, Measuring the boiling point of the vacuum of quantum electrodynamics, Phys. Rev. D **99**, 036008 (2019).
[17] S. Villalba-Chávez and C. Müller, Photo-production of scalar particles in the field of a circularly polarized laser beam, Phys. Lett. B **718**, 992 (2013).
[18] M. J. A. Jansen and C. Müller, Strongly enhanced pair production in combined high- and low-frequency laser fields, Phys. Rev. A **88**, 052125 (2013).
[19] K. Krajewska and J. Z. Kamiński, Coherent combs of antimatter from nonlinear electron-positron-pair creation, Phys. Rev. A **90**, 052108 (2014).
[20] S. Meuren, C. H. Keitel, and A. Di Piazza, Semiclassical picture for electron-positron photoproduction in strong laser fields, Phys. Rev. D **93**, 085028 (2016).
[21] T. G. Blackburn and M. Marklund, Nonlinear Breit-Wheeler pair creation with bremsstrahlung γ rays, Plasma Phys. Controlled Fusion **60**, 054009 (2018).
[22] A. I. Titov and B. Kämpfer, Non-linear Breit-Wheeler process with linearly polarized beams, Eur. Phys. J. D **74**, 218 (2020).
[23] C. Baumann, E. N. Nerush, A. Pukhov, and I. Yu. Kostyukov, Probing nonperturbative QED with electron-laser collisions, Sci. Rep. **9**, 9407 (2019).
[24] C. Baumann and A. Pukhov, Laser-solid interaction and its potential for probing radiative corrections in strong-field quantum electrodynamics, Plasma Phys. Controlled Fusion **61**, 074010 (2019).
[25] T. G. Blackburn, A. Ilderton, M. Marklund, and C. P. Ridgers, Reaching supercritical field strengths with intense lasers, New J. Phys. **21**, 053040 (2019).
[26] A. Di Piazza, T. N. Wistisen, M. Tamburini, and U. I. Uggerhøj, Testing Strong Field QED Close to the Fully Nonperturbative Regime using Aligned Crystals, Phys. Rev. Lett. **124**, 044801 (2020).
[27] V. Yakimenko *et al.*, Prospect of Studying Nonperturbative QED with Beam-Beam Collisions, Phys. Rev. Lett. **122**, 190404 (2019).
[28] V. I. Ritus, Radiative effects and their enhancement in an intense electromagnetic field, Zh. Eksp. Teor. Fiz. **57**, 2176 (1969) [J. Exp. Theor. Phys. **30**, 1182 (1970)].
[29] A. A. Mironov, S. Meuren, and A. M. Fedotov, Resummation of QED radiative corrections in a strong constant crossed field, Phys. Rev. D **102**, 053005 (2020).
[30] T. Podszus and A. Di Piazza, High-energy behavior of strong-field QED in an intense plane wave, Phys. Rev. D **99**, 076004 (2019).
[31] A. Ilderton, Note on the conjectured breakdown of QED perturbation theory in strong fields, Phys. Rev. D **99**, 085002 (2019).
[32] D. L. Burke *et al.*, Positron Production in Multiphoton Light-by-Light Scattering, Phys. Rev. Lett. **79**, 1626 (1997).
[33] B. King, H. Gies, and A. Di Piazza, Pair production in a plane wave by thermal background photons, Phys. Rev. D **86**, 125007 (2012).
[34] O. J. Pike, F. Mackenroth, E. G. Hill, and S. J. Rose, A photon-photon collider in a vacuum hohlraum, Nat. Photonics **8**, 434 (2014).
[35] X. Ribeyre, E. d'Humières, O. Jansen, S. Jequier, V. T. Tikhonchuk, and M. Lobet, Pair creation in collision of γ-ray beams produced with high-intensity lasers, Phys. Rev. E **93**, 013201 (2016).
[36] I. Drebot *et al.*, Matter from light-light scattering via Breit-Wheeler events produced by two interacting Coulomb sources, Phys. Rev. Accel. Beams **20**, 043402 (2017).
[37] T. Wang, X. Ribeyre, Z. Gong, O. Jansen, E. d'Humières, D. Stutman, T. Toncian, and A. Arefiev, Power Scaling for Collimated γ-Ray Beams Generated by Structured Laser-Irradiated Targets and Its Application to Two-Photon Pair Production, Phys. Rev. Applied **13**, 054024 (2020).
[38] A. Golub, S. Villalba-Chávez, H. Ruhl, and C. Müller, Linear Breit-Wheeler pair production by high-energy bremsstrahlung photons colliding with an intense X-ray laser pulse, Phys. Rev. D **103**, 016009 (2021).
[39] H. Abramowicz *et al.*, Letter of intent for the LUXE experiment, arXiv:1909.00860.
[40] The E-320 experiment of the FACET-II initiative at SLAC aims to measure the nonperturbative Breit-Wheeler process; https://portal.slac.stanford.edu/.
[41] For Schwinger effect in bandgapped graphene, see I. Akal, R. Egger, C. Müller, and S. Villalba-Chávez, Low-dimensional approach to pair production in an oscillating electric field: Application to bandgap graphene layers, Phys. Rev. D **93**, 116006 (2016); Simulating dynamically assisted production of Dirac pairs in gapped graphene monolayers, Phys. Rev. D **99**, 016025 (2019).
[42] For Schwinger effect and other pair production-related phenomena in gapless graphene, we refer to D. Allor, T. D. Cohen, and D. A. McGady, Schwinger mechanism and graphene, Phys. Rev. D **78**, 096009 (2008); G. N. Klimchitskaya and V. M. Mostepanenko, Creation of quasiparticles in graphene by a time-dependent electric field, Phys. Rev. D **87**, 125011 (2013); F. Fillion-Gourdeau and S. MacLean, Time-dependent pair creation and the Schwinger mechanism in graphen, Phys. Rev. B **92**, 035401 (2015); F. Fillion-Gourdeau, D. Gagnon, C. Lefebvre, and S. MacLean, Time-domain quantum interference in graphene, Phys. Rev. B **94**, 125423 (2016); S. P. Gavrilov, D. M. Gitman, and N. Yokomizo, Dirac fermions in strong electric field and quantum transport in graphene, Phys. Rev. D **86**, 125022 (2012); H. K. Avetissian, A. K. Avetissian, G. F. Mkrtchian, and K. V. Sedrakian, Multiphoton resonant excitation of Fermi-Dirac sea in graphene at the interaction with strong laser fields, J. Nanophoton. **6**, 061702 (2012); M. C. Suster, J. Derlikiewicz, K. M. Kotur, F. Cajiao Vélez, K. Krajewska, and J. Z. Kamiński, Dynamical mass generation in graphene by bicircular laser fields, J. Phys. Conf. Ser. **1508**, 012004 (2020).
[43] A. Golub, R. Egger, C. Müller, and S. Villalba-Chávez, Dimensionality-Driven Photoproduction of Massive Dirac

Pairs near Threshold in Gapped Graphene Monolayers, Phys. Rev. Lett. **124**, 110403 (2020).
[44] L. Fister, R. Alkofer, and K. Schwenzer, On the infrared behavior of Landau Gauge Yang-Mills theory with a fundamentally charged scalar field, Phys. Lett. B **688**, 237 (2010).
[45] T. Banks and M. O'Loughlin, Two-dimensional quantum gravity in Minkowski space, Nucl. Phys. **B362**, 649 (1991).
[46] S. Desser, R. Jakiw, and S. Templeton, Topologically massive gauge theories, Ann. Phys. (N.Y.) **140**, 372 (1982).
[47] R. Prange and S. Girvin, *The Quantum Hall Effect* (Springer-Verlag, New York, 1990).
[48] Q. Lin, Electron-positron pair creation in a vacuum by an electromagnetic field in $3+1$ and lower dimensions, J. Phys. G **25**, 17 (1999).
[49] S. P. Gavrilov and D. M. Gitman, Vacuum instability in external fields, Phys. Rev. D **53**, 7162 (1996).
[50] Y. Lu, N. Christensen, Q. Su, and R. Grobe, Space-time-resolved Breit-Wheeler process for a model system, Phys. Rev. A **101**, 022503 (2020).
[51] Q. Z. Lv, N. D. Christensen, Q. Su, and R. Grobe, Validity of one-dimensional QED for a system with spatial symmetry, Phys. Rev. A **92**, 052115 (2015).
[52] E. A. Martinez *et al.*, Real-time dynamics of lattice gauge theories with a few-qubit quantum computer, Nature (London) **534**, 516 (2016).
[53] A. N. Pieiro, D. Genkina, M. Lu, and I. B. Spielman, Sauter-Schwinger effect with a quantum gas, New J. Phys. **21**, 083035 (2019).
[54] N. Szpak and R. Schützhold, Quantum simulator for the Schwinger effect with atoms in bichromatic optical lattices, Phys. Rev. A **84**, 050101(R) (2011).
[55] N. Szpak and R. Schützhold, Optical lattice quantum simulator for quantum electrodynamics in strong external fields: spontaneous pair creation and the Sauter-Schwinger effect, New J. Phys. **14**, 035001 (2012).
[56] T. Pichler, M. Dalmonte, E. Rico, P. Zoller, and S. Montangero, Real-Time Dynamics in U(1) Lattice Gauge Theories with Tensor Networks, Phys. Rev. X **6**, 011023 (2016).
[57] E. Zohar, A. Farace, B. Reznik, and J. Ignacio Cirac, Digital Quantum Simulation of Z_2 Lattice Gauge Theories with Dynamical Fermionic Matter, Phys. Rev. Lett. **118**, 070501 (2017).
[58] T. V. Zache *et al.*, Quantum simulation of lattice gauge theories using Wilson fermions, Quantum Sci. Technol. **3**, 034010 (2018).
[59] L. Klar, N. Szpak, and R. Schützhold, Quantum simulation of spontaneous pair creation in 2D optical lattices, arXiv:1901.09880.
[60] R. Ott, T. V. Zache, N. Mueller, and J. Berges, Non-cancellation of the parity anomaly in the strong-field regime of QED_{2+1}, Phys. Lett. B **805**, 135459 (2020).
[61] J. M. Guilarte and M. de la Torre Mayado, QED_{2+1}: The Compton effect, An. Fis. (Spain) **6**, 237 (2002), arXiv:hep-th/0009003.
[62] S Bellucci, A. A. Saharian, and V. M. Bardeghyan, Induced fermionic current in toroidally compactified spacetimes with applications to cylindrical and toroidal nanotubes, Phys. Rev. D **82**, 065011 (2010).
[63] D. M. Volkov, On a class of solutions of the Dirac equation, Z. Phys. **94**, 250 (1935).
[64] V. B. Berestetskii, E. M. Lifshitz, and L. P. Pitaevskii, *Relativistic Quantum Theory* (Pergamon Press Ltd., Oxford, 1971).
[65] H. R. Reiss, Effect of an intense electromagnetic field on a weakly bound system, Phys. Rev. A **22**, 1786 (1980).
[66] V. P. Krainov, H. R. Reiss, and B. M. Smirnov, *Radiative Processes in Atomic Physics* (John Wiley and Sons, New York, 1997).
[67] F. W. J. Olver, D. W. Lozier, R. F. Boisvert, and C. W. Clark, *NIST Handbook of Mathematical Functions* (Cambridge University Press, Cambridge, England, 2010).
[68] I. S. Gradshtein and I. M. Ryzhik, *Table of Integrals, Series, and Products (Sixth Edition)* (Academic Press, New York, 2000).
[69] M. J. Ablowitz and A. S. Fokas, *Complex Variables: Introduction and Applications* (Cambridge University Press, Cambridge, England, 2003).
[70] C. Leubner, Uniform asymptotic expansion of a class of generalized Bessel functions occuring in the study of fundamental scattering processesin intense laser fields, Phys. Rev. A **23**, 2877 (1981).
[71] D. E. Aspnes, Electric-field effects on optical absorption near threshold in solids, Phys. Rev. **147**, 554 (1966).
[72] W. Greiner and J. Reinhardt, *Quantum Electrodynamics* (Springer-Verlag, Berlin, Heidelberg, 2003).